Inorg. Chem. **2009**, *48*, 1967−1973

Observation of the Ammonium Salt of 12-Molybdophosphoric Acid by in Situ Raman Spectroscopy during Solid-State Synthesis: Spectral Analysis and Reconstruction Using the Band-Target Entropy Minimization (BTEM) Algorithm

Chilukoti Srilakshmi,* Wee Chew, Kanaparthi Ramesh, and Marc Garland*

Institute of Chemical and Engineering Sciences (ICES), 1, Pesek Road, Jurong Island, Singapore, 627833

Received August 24, 2008

The solid-state reaction between ammonium heptamolybdate (AHM) and zirconium phosphate (ZrP) to give the ammonium salt of 12-molybdophosphoric acid (AMPA) was performed at 25−400 °C and monitored using in situ Raman spectroscopy. Spectral analysis of the Raman data using the band-target entropy minimization (BTEM) algorithm resulted in spectral estimates for the starting materials and product, AHM, ZrP, and AMPA, as well as the byproduct MoO_3 and an intermediate $11(NH_4)_2O \cdot 4(MoO_3)_7$. The time-dependent relative concentration profiles were obtained, and the contributions of the individual signal intensities of each constituent to the total measured signal intensity were determined (range: 8.4−27.2%). The present results are important since the synthesis of AMPA is normally performed in buffered aqueous solution and not in the solid state. The present study also indicates that a maximum yield of the desired ammonium salt of 12-molybdophosphoric acid is achieved by stopping the solid-state reaction at ca. 350 °C. The combined spectroscopic and chemometric approach used in this contribution appears applicable to other solid-state synthetic studies in order to reveal more detailed time-dependent information on the species present.

1. Introduction

12-Molybdophosphoric acid (MPA), an important heteropolycompound, has been extensively used as a catalyst for a variety of chemical reactions.[1] Bulk MPA exhibits the well-known Keggin structure[2] with 12 edge-sharing molybdenum(VI) MoO_6 octahedra surrounding the central PO_4 tetrahedron. In spite of the importance of MPA as a catalyst, its wider application is restricted because of its complexity, poor reproducibility of the methods of synthesis, and low thermal stability. These drawbacks limit the practical application of MPA. For example, apart from the calcination temperature, the rate at which this temperature is reached also affects the final structure.[3] In order to overcome these difficulties, several methods have been reported for the preparation of the salts of heteropolyacid exhibiting the Keggin structure. Two of the important routes are (1) dissolution of the appropriate amounts of the precursors, that is, HPA and ammonium carbonate/nitrate in water, followed by precipitation at controlled pH, and the extraction of the solvent,[4] and (2) direct precipitation by dissolution of the appropriate amounts of the cations in the solution containing the dissolved acids.[5]

We previously reported an alternate synthesis, by interacting the phosphate ion of the metal phosphate with molybdenum species of the AHM, thus avoiding corrosive reagents such as H_3PO_4.[6−9] A few other studies have also reported the formation of heteropoly compounds by reacting the fluid

* To whom correspondence should be addressed. E-mail: c_srilakshmi@ices.a-star.edu.sg (C.S.), marc_garland@ices.a-star.edu.sg (M.G.).

(1) Mizuno, N.; Misono, M. *Chem. Rev.* **1998**, *98*, 199.
(2) Kozhevnikov, I. V. *Chem. Rev.* **1998**, *98*, 171.
(3) Albonetti, S.; Cavani, F.; Trifiro, F.; Gazzano, M.; Koutyrev, M.; Aissi, F. C.; Aboukais, A.; Guelton, M. *J. Catal.* **1994**, *146*, 491.
(4) McGarvey, G. B.; Moffat, J. B. *J. Catal.* **1991**, *130*, 483.
(5) Van Veen, J. A. R.; Hendriks, P. A. J. M.; Andrea, R. R.; Romers, E. J. G. M.; Wilson, A. E. *J. Phys. Chem.* **1990**, *94*, 5282.
(6) Sai Prasad, P. S.; Raghavan, K. V.; Suryanarayana, I.; Rao, K. N.; Srilakshmi, C.; Santosh kumar, M.; Reddy, K. B. U.S. Patent 6,534,435, 2003.
(7) Srilakshmi, C.; Narasimha Rao, K.; Lingaiah, N.; Suryanarayana, I.; Sai Prasad, P. S. *Catal. Lett.* **2002**, *83*, 127.
(8) Srilakshmi, C.; Ramesh, K.; Anderson, B. G.; Niemantsverdriet, J. W.; Sai Prasad, P. S. *Appl. Catal. A* **2005**, *296*, 54.
(9) Srilakshmi, C.; Lingaiah, N.; Sai prasad, P. S.; Narayana, K. V.; Martin, A.; Lucke, B. *Catal. Commun.* **2004**, *5*, 199.

10.1021/ic801609d CCC: $40.75
Published on Web 01/12/2009

phase with one or more of the species in the solid phase.[10,11] Hence, it is interesting to examine the possibility of generating the salts of MPA, in their Keggin structure, by solid−solid interaction between a phosphate support and a molybdenum salt.

In addition, in situ Raman spectroscopy of this solid-state reaction can provide interesting information concerning the reaction chemistry. Indeed, Raman spectroscopy has, over the past few years, contributed to considerable progress in the area of heterogeneous catalysis because of its in situ capabilities and its ability to identify different metal oxide structures. The novelty of the present investigation is the formation of the ammonium salt of MPA (AMPA), by solid−solid interaction between $(NH_4)_6Mo_7O_{24}\cdot 4H_2O$ and zirconium phosphate, and the use of advanced chemometric techniques in order to better understand the solid-state syntheses. In this manner, issues pertaining to pH control are avoided. To the best of our knowledge, this approach had not been previously reported.

With regard to the solid-state reaction chemistry, we have successfully applied band-target entropy minimization (BTEM) spectral reconstruction methods to the in situ Raman data in order to reconstruct the pure component spectra of the components observed during the AMPA formation. BTEM is a self-modeling curve resolution computational method that has recently been developed. It has been shown to be capable of separating the spectra of "pure components" from matrices of mixture spectra[12−18] without any recourse to a priori information such as spectral libraries. The BTEM algorithm has been successfully applied to the analysis of data matrices generated by a number of different spectroscopic techniques including IR, infrared reflection absorption spectroscopy, X-ray diffraction (XRD), NMR, and FT-Raman.[19−23] Although originally developed for vibrational spectroscopic studies of liquid-phase reactions, BTEM has recently been applied to heterogeneously catalytic systems. Thus, application of BTEM to DRIFTS data from CO and NO adsorption studies on Pt and Pd has resulted in the reconstruction of pure component spectra of minor species,

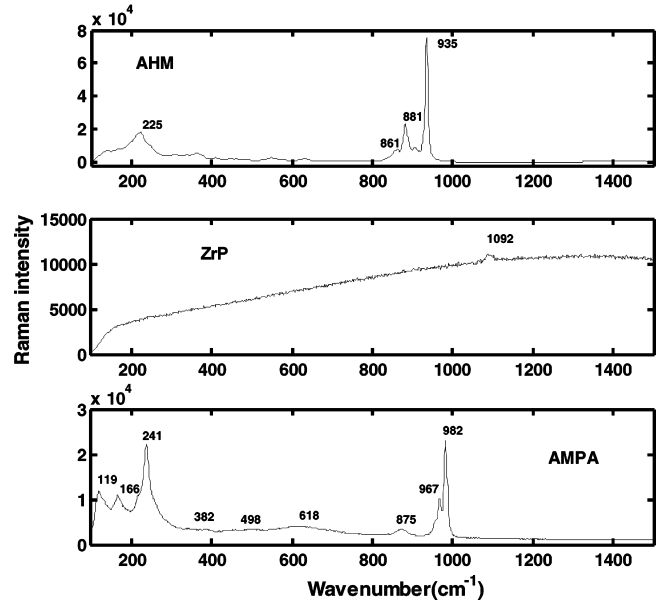

Figure 1. Reference Raman spectra of the starting complexes and product ammonium heptamolybdate, zirconium phosphate, and AMPA used in this study.

that is, those having less than 0.05% of the total signal intensity such as isocyanate species.[24−26] In addition, some previously unreported species were identified.

The present study represents the first application of in situ Raman spectroscopic data and BTEM analysis to study a solid-state synthesis. These experiments cover a variety of temperatures and resulted in the reconstruction of the pure component spectra obtained during solid-state reaction between AHM and ZrP. It appears that the present combined approach should be applicable to the study of other solid-state syntheses.

2. Experimental Methods

Zirconium phosphate (P/Zr ratio of 2.0) was prepared by adding zirconium nitrate to a vigorously stirred aqueous solution of HCl (2 mol) and H_3PO_4 (4 mol) to yield a gelatinous precipitate which was washed with 2% H_3PO_4 (aq). Upon drying the sample at 120 °C overnight, amorphous ZrP was obtained. The obtained amorphous ZrP was calcined at 400 °C for 4 h. Ammonium heptamolybdate (Sigma-Aldrich) with a purity of 99.98% was used without any further purification. Purified air was used during the solid-state reactions (ca. 99.98% Soxal, Singapore). The measured reference Raman spectra of the starting complexes are shown in Figure 1.

The in situ Raman study involved two different initial ratios of reagents, namely, (1) AHM/ZrP = 0.7 and (2) AHM/ZrP = 1.0. The solids were mixed thoroughly using a mortar and pestle to a fine powder and loaded into the in situ Raman cell (Linkam Model CCR 1000, U.K.) fitted with ZnSe windows for measurements.

2.1. Raman Microscopy. Raman spectra were measured using a Raman microscope (In Via Reflex, Reni-Shaw) equipped with a Peltier cooled deep-depleted CCD array detector (576 × 384 pixels) and a high grade Leica microscope. The Raman scattering was

(10) Kasztelan, S.; Payen, E.; Moffat, J. B. *J. Catal.* **1988**, *112*, 320.
(11) Banares, M. A.; Fierro, J. L. G.; Moffat, J. B. *J. Catal.* **1993**, *142*, 406.
(12) Chew, W.; Widjaja, E.; Garland, M. *Organometallics.* **2002**, *21*, 1982.
(13) Li, C.; Widjaja, E.; Chew, W.; Garland, M. *Angew. Chem., Int. Ed.* **2002**, *41*, 3785.
(14) Li, C.; Widjaja, E.; Garland, M. *J. Am. Chem. Soc.* **2003**, *125*, 5540.
(15) Widjaja, E.; Li, C.; Chew, W.; Garland, M. *Anal. Chem.,* **2003**, *75*, 4499.
(16) Widjaja, E.; Crane, N.; Chen, T.-S.; Morris, M. D.; Ignelzi, M. A., Jr.; McCreadie, B. R. *Appl. Spectrosc.* **2003**, *57*, 1353.
(17) Srilakshmi, Ch.; Widjaja, E.; Anderson, B. G.; Garland, M. *Talanta* **2007**, *72*, 847.
(18) Srilakshmi, Ch.; Widjaja, E.; Garland, M.; Anderson, B. G. *J. Raman. Spectrosc.* **2007**, *38*, 349.
(19) Liangfeng, G.; Kooli, F.; Garland, M. *Anal. Chim. Acta* **2004**, *517*, 229.
(20) Liangfeng, G.; Wiesmath, A.; Sprenger, P.; Garland, M. *Anal. Chem.* **2005**, *77*, 655.
(21) Ong, L. R.; Widjaja, E.; Stanforth, R.; Garland, M. *J. Raman Spectrosc.* **2003**, *34*, 282.
(22) Cheng, S.; Rajarathnam, D.; Meiling, T.; Garland, M. *Appl. Spectrosc.* **2006**, *60* (5), 521.
(23) Boon Hong, K.; Wee-Sun, S.; Chew, W. *Anal. Chim. Acta* **2006**, *571* (1), 113.
(24) Li, C.; Widjaja, E.; Garland, M. *J. Catal.* **2003**, *213*, 126.
(25) Srilakshmi, C.; Widjaja, E.; Feng, G.; Huajun, Z.; Anderson, B. G.; Hans Niemantsverdriet, J. W. *Phys. Chem. Chem. Phys.,* **2008**, *10*, 3535.
(26) Srilakshmi, C.; Feng, G.; Anderson, B. G.; Hans Niemantsverdriet, J. W. *Phys. Chem. Chem. Phys.* **2008**, *10*, 5510.

excited with a red laser (785 nm), and a 20× objective lens was used to collect the backscattered light. A spot size of ca. 2 μm was used. All of the spectra were acquired with a laser power of ca. 111−230 μW with an exposure time of 10 s over the range of 100−1500 cm^{-1}.

2.2. In Situ Raman Spectroscopic Studies. A 30 mg sample of powder (AHM and ZrP) mixed thoroughly in an agate mortar was loaded into the in situ Raman cell, and the temperature was raised from room temperature (Rt) to 400 °C in a purified air flow of 20 mL/min. The temperature was increased in 50 °C intervals at a rate of 10 °C/min and then held constant for ca. 30 min. This was repeated until the final temperature of 400 °C was reached. The sample was kept isothermal for another 120 min at 400 °C.

In experiment 1 with AHM/ZrP = 0.7, 33 spectra were acquired, and in experiment 2 with AHM/ZrP = 1.0, 62 spectra were acquired.

3. Computational Aspects

3.1. Band-Target Entropy Minimization (BTEM) Algorithm. As previously mentioned, the primary use of BTEM is to extract the pure component spectra from a set of multicomponent mixture spectra, without recourse to a priori information of any kind, including spectral libraries. Afterward, the contributions of each individual pure component spectrum to the measured experimental spectra can be determined using multilinear regression in order to estimate the signal contribution of each species as well as the relative concentrations.

Let $\mathbf{I}_{k\times\nu}$ represent the Raman intensity in the consolidated spectroscopic data matrix, where k denotes the number of spectra taken and ν denotes the number of data channels associated with the spectroscopic range. The experimental intensities $\mathbf{I}_{k\times\nu}$ have a bilinear data structure and can be described as a product of two matrices, namely, the concentration matrix $\mathbf{C}_{k\times s}$ and the Raman pure component scattering coefficient matrix $\mathbf{J}_{s\times\nu}$ (where s denotes the number of observable species in the chemical mixture). Accordingly, the associated error matrix $\boldsymbol{\varepsilon}_{k\times\nu}$ contains both experimental error and model error (nonlinearities).[27]

$$\mathbf{I}_{k\times\nu} = \mathbf{C}_{k\times s}\mathbf{J}_{s\times\nu} + \boldsymbol{\varepsilon}_{k\times\nu} \tag{1}$$

The BTEM algorithm proceeds by first decomposing $\mathbf{I}_{k\times\nu}$ into its singular vectors using singular value decomposition (SVD), as shown in eq 2.[28] This is then followed by the appropriate transformation of the right singular vectors, $\mathbf{V}^{\mathrm{T}}$, into physically meaningful pure component spectra. See section 4.2.1 for more details.

$$\mathbf{I}_{k\times\nu} = \mathbf{U}_{k\times k}\boldsymbol{\Sigma}_{k\times\nu}\mathbf{V}^{\mathrm{T}}_{\nu\times\nu} \tag{2}$$

In contrast to other self-modeling curve resolution methods, BTEM was uniquely developed to resolve one pure component spectrum at a time. The number of right singular vectors, z, taken for inclusion in the transformation, is usually much larger than s, to account for any nonlinearities present (nonstationary spectral characteristics). The number z is usually determined by identifying the vectors which possess localized spectral bands or features of clear physical significance and retaining these, while discarding the vectors that are associated with randomly distributed noise. The principal

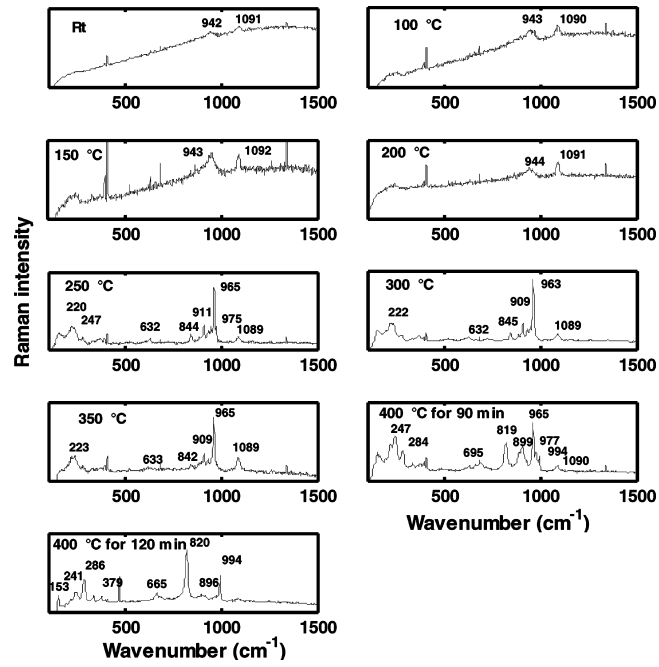

Figure 2. Selected in situ Raman spectra of the solid-state reaction of ammonium heptamolybdate and zirconium phosphate at various temperatures.

equation representing the transformation of the right singular vectors into each spectral estimate is given by eq 3, where $\hat{\mathbf{J}}_{1\times\nu}$ is the BTEM estimated pure component Raman spectrum, $\mathbf{T}_{1\times z}$ is the transformation vector, and $\mathbf{V}^{\mathrm{T}}{}_{z\times\nu}$ is the set of basis vectors used as the basis set.

$$\hat{\mathbf{J}}_{1\times\nu} = \mathbf{T}_{1\times z}\mathbf{V}^{\mathrm{T}}_{z\times\nu} \tag{3}$$

Each pure Raman spectral estimate $\hat{\mathbf{J}}_{1\times\nu}$ is obtained by targeting bands in the first few $\mathbf{V}^{\mathrm{T}}$ vectors. The BTEM algorithm then retains this selected feature and, at the same time, returns an entire spectrum which has minimum entropy. Accordingly, the resulting spectral estimate is the simplest pattern present. This procedure is repeated for all important observable physical features in the selected $\mathbf{V}^{\mathrm{T}}$ vectors. A superset of reconstructed pure component spectra is obtained. This superset is then reduced to a smaller set of representative spectral patterns to eliminate spectral redundancies. This results in an enumeration of all observable pure component spectra.

In the present study, a total of 95 spectra were measured, 33 in the first experimental run and then 62 in the second experiment. The combined intensity matrix had dimensions $\mathbf{I}_{95\times1414}$.

4. Results and Discussion

4.1. Raman Spectroscopy. Some selected and representative in situ Raman spectra from the solid-state reaction between AHM and ZrP, measured at various temperatures, are presented in Figure 2. These spectra show that some considerable baseline shifts occur. The low-temperature spectra show some relatively significant background or fluorescence. Above ca. 250 °C, this background more-or-less disappears. In addition, spikes (due to cosmic rays) can be seen in a few of the spectra. Clearly, there is considerable change in the prominent Raman bands as the solid-state reaction proceeds.

(27) Garland, M.; Visser, E.; Terwiesch, P.; Rippin, D. W. T. *Anal. Chim. Acta* **1997**, *35*, 1337.
(28) Golub G. H.; Van Loan, C. F. *Matrix Computations*; Johns Hopkins University Press: Baltimore, 1996.

Spectra measured of the initial powder mixture at Rt showed bands at 1091 and 943 cm^{-1}. The peak at 1091 corresponds to ZrP, and the peak at 943 cm^{-1} corresponds to $11(NH_4)_2O\cdot4(MoO_3)_7$. The latter was apparently generated during the solid-phase grinding and sample preparation. $11(NH_4)_2O\cdot4(MoO_3)_7$ is one of the intermediates found during the thermal decomposition of ammonium heptamolybdate to MoO_3 using Raman spectroscopy by Murugan and Chang.[29] A similar type of intermediate has been observed by others using IR, XRD, and thermogravimetric−differential thermal analysis.[30−33] There are no significant changes observed in the spectra measured from 100 to 200 °C.

The spectra observed from 250−400 °C indicated major changes. At 250 °C, the spectra show a mixture of phases containing both AMPA at 1089, 975, 965, 920, 911, 887, 632, and 247 cm^{-1} and less intense bands of $11(NH_4)_2O\cdot4(MoO_3)_7$ at 945, 932, 844, and 220 cm^{-1}. It can be seen that the band at 942 cm^{-1} for $11(NH_4)_2O\cdot4(MoO_3)_7$ shifts to 945 cm^{-1} as the temperature is increased from Rt to 250 °C. Salts of heteropolyacids can be present as aggregates of mono-oxo species. The main spectroscopic features of AMPA having a Keggin structure were observed at 1089 cm^{-1} (ν_{as} P−O, weak), 975 cm^{-1} (ν_s Mo−O_d), 965 cm^{-1} (ν_{as} Mo−O_d), 920−877 cm^{-1} (ν_{as} Mo−Ob−Mo), 632 cm^{-1}(ν_{as} Mo−Oc−Mo), and 247 cm^{-1} (νs Mo−Oa). The spectral features observed for ZrP, $11(NH_4)_2O\cdot4(MoO_3)_7$, and AMPA agree with those reported in the literature.[29,34−36] A summary of the observed bands and their assignments are given in Table 1. Above 300 °C, bands corresponding to $11(NH_4)_2O\cdot4(MoO_3)_7$ disappear, and bands due to AMPA continue to increase up to 400 °C.

AMPA was stable at 400 °C for ca. 30−40 min and then started to decompose to hexagonal MoO_3, which shows bands at 899 and 695 cm^{-1}. With increasing time, hexagonal MoO_3 was completely transformed into orthorhombic MoO_3, which shows peaks at 820, 994, 663, and 285 cm^{-1}. This can be seen in Figure 2 from the spectrum at 400 °C with a 120 min reaction time. It is important to note that a replicate experiment gave similar spectra.

4.2. Pure Component Spectral Reconstruction. 4.2.1. Singular Value Decomposition. The 95 raw Raman mixture spectra from the combined experiments were subjected to a singular value decomposition, yielding two orthonormal matrices $\mathbf{U}_{95\times95}$ and $\mathbf{V}^T_{1414\times1414}$ and the diagonal singular value matrix $\mathbf{\Sigma}_{95\times1414}$. The row vectors of the $\mathbf{V}^T$ matrix (normally called the right singular vectors) represent a set of basis vectors which contain abstract information on the pure component spectra of the observable components present in the system. These basis vectors are ordered according to their contribution to the total variance in the observations. Hence, the initial few vectors are associated with the chemically significant information in the system, and the remaining vectors are primarily associated with the random instrumental error. In addition, it should be noted that, after decomposition, there are a total of 1414 basis vectors in $\mathbf{V}^T$, but only 95 vectors are physically meaningful (possessing either chemical or random error signals). This is due to the fact that there are only 95 spectra in the original data set.

Since not all 95 right singular vectors are needed in further analysis (many of the last vectors are primarily noise), the set of vectors can be reduced, and only a subset will be used in the BTEM spectral reconstructions. Figure 3 shows some of the first 20 right singular vectors. The first two vectors show many localized signals superimposed on large background signals. The next eight vectors have clear localized signals, but this is often accompanied by a wavy baseline (see vector 8). Vectors 11−20 are primarily noise, but they are heteroscedasticly distributed. The remaining vectors were essentially white noise. Accordingly, 20 $\mathbf{V}^T$ right singular vectors were used in the subsequent BTEM spectral reconstructions.

4.2.3. Spectral Reconstruction. It is known that, if all of the chemically significant extrema (minima and maxima) in the primary right singular vectors are targeted, then a superset of observable pure component spectra are obtained, in which many replicates appear. This is the approach that has been

Table 1. Characteristic Raman Peak Assignments of the Species Observed in the Present Study[8,29−38]

Species	Raman shift	assignment
AHM	935	ν(Mo−O)
	902	
	892	
	885	
	859	ν(Mo−O−Mo)
	840	ν(Mo−O−Mo)
ZrP	1091	ν(P−O)
$11(NH_4)_2O\cdot4(MoO_3)_7$	945	ν(Mo−O)
	932	
	844	ν(Mo−O−Mo)
AMPA	975, 965	νs(Mo−Od)
	920−877	ν_{as}(Mo−Od)
	632	ν_{as}(Mo−Ob−Mo)
	247	νs(Mo−Oa) with bridging character
MoO_3 (orthorhombic)	994	ν_{as}(O═Mo═O) twist
	820	ν_s(O═Mo═O) twist
	663	ν(O−Mo−O)
	471	ν Mo−O−Mo stretch and bend
	378	δ(O═Mo═O) scissors
	338	δ(Mo−O−Mo) bend
	285	δ(O═Mo═O) wagging
	243	τ_s(O═Mo═O) twist
MoO_3 (hexagonal)	977	ν(OMo)
	899	corner modes of ν (Mo−O−Mo)
	882	
	695	edge mode of ν (OMo_3)
	283	$\delta(OMo_3)$
	248	$\delta(OMo_2)$
	220	$\delta(OMo_2)$

(29) Murugan, R.; Chang, H. *J. Chem. Soc., Dalton Trans.* **2001**, 3125.
(30) Hanafi, Z. M.; Khilla, M. A.; Askar, M. H. *Thermochim. Acta* **1981**, *45*, 221.
(31) Zhoulan, Y.; Xinhai, L.; Qiyuam, C. *Thermochim. Acta* **2000**, *352*, 107.
(32) Ma, E. *Bull. Chem. Soc. Jpn.* **1964**, *37*, 171.
(33) Ma, E. *Bull. Chem. Soc. Jpn.* **1964**, *37*, 648.
(34) Rocchiccioli-Deltcheff, C.; Aouissi, A.; Bettahar, M. M.; Launay, S.; Fournier, M. *J. Catal.* **1996**, *164*, 16.
(35) Kasprzak, M. S.; Crouch, S. R.; Leroi, G. E. *Appl. Spectrosc.* **1978**, *32*, 537.
(36) Cavani, F.; Etienne, E.; Mezzogori, R.; Pigamo, A.; Trifiro, F. *Catal. Lett.* **2001**, *75*, 99.
(37) Mestl, G.; Ilkenhans, T.; Spielbauer, D.; Dieterle, M.; Timpe, O.; Kröhnert, J.; Jentoft, F.; Knözinger, H.; Schlögl, R. *Appl. Catal.* **2001**, *210*, 13.
(38) Yurchenko, E. N. *J. Struct. Chem.* **1987**, *28*, 446.

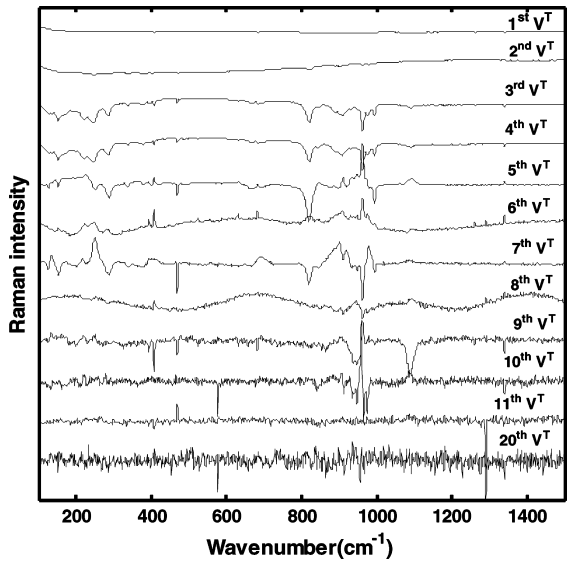

Figure 3. Some of the first 20 $\mathbf{V}^T$ vectors obtained by SVD.

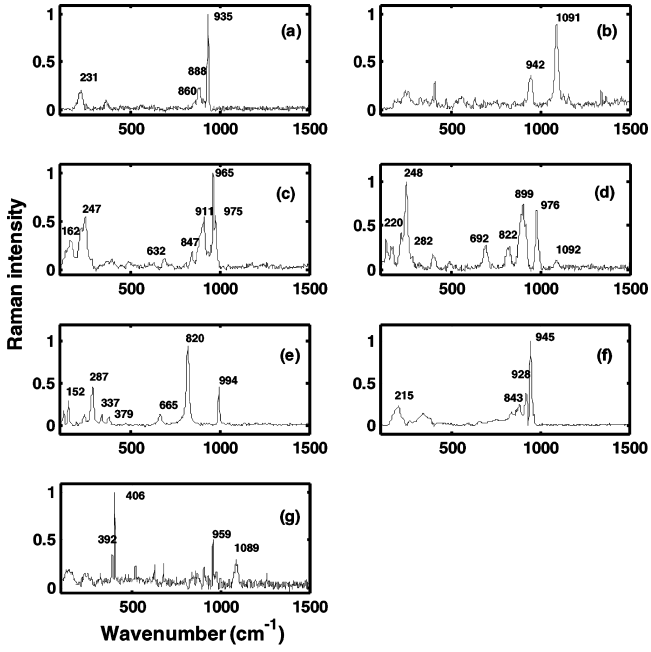

Figure 4. The results for the BTEM analysis for the full-range spectral patterns. (a) AHM, (b) ZrP, (c) AMPA $[(NH_4)_3PMo_{12}O_{40}\cdot 4H_2O]$, (d) hexagonal MoO_3, (e) orthorhombic MoO_3, (f) $11(NH_4)_2O\cdot 4(MoO_3)_7$, (g) visible light.

taken with FTIR for new chemically reactive liquid phase systems with an unknown number of new and previously unobserved species. In the present test for a solid-phase reaction, a similar approach is taken. Accordingly, from the first 10 $\mathbf{V}^T$ vectors, significant spectral features were selected as band targets in the spectral reconstructions, and exhaustive searches of the data were performed.

4.2.3.1. Full-Range Analysis. BTEM was applied to the full spectral range 100−1500 cm^{-1} in order to obtain pure component spectral estimates. A total of seven distinct patterns were reconstructed, as shown in Figure 4. Six of these patterns correspond to inorganic species, while that last pattern corresponds to stray light captured by the measurements. Relatively good spectral estimates are obtained for the starting materials AHM, with a maximum at 935 cm^{-1} (Figure 4a), and ZrP, with maximum at 1090 cm^{-1} (Figure 4b) (please compare spectral estimates and relative intensities of bands to references in Figure 1).

The remaining four spectral estimates are assigned to AMPA with a maximum at 965 cm^{-1} (Figure 4c),[8,37] hexagonal MoO_3 at 899 cm^{-1} (Figure 4d),[38] orthorhombic MoO_3 (Figure 4e) with maximum at 820 cm^{-1},[38] and $11(NH_4)_2O\cdot 4(MoO_3)_7$ with a maximum at 945 cm^{-1} (Figure 4f).[29] It should be noted that some of the full-range pure component spectral estimates shown in Figure 4 contain small signal artifacts, as well as a moderate level of noise.

4.2.3.2. Partial Range Analysis. The full range BTEM estimates were of sufficiently good quality for identification purposes. However, for quantitative analysis, it is frequently advantageous to repeat the BTEM analysis over a restricted spectral range. This usually results in significantly improved signal-to-noise ratios as well as the suppression of most artifacts.

The region 600−1300 cm^{-1} was selected for the partial range analysis since this region contains numerous bands for all of the species present. The BTEM analysis resulted in considerably improved signal-to-noise ratios for all of the constituent spectra. In addition, these pure component spectral estimates were then mapped back onto a *baseline-corrected* data set in order to determine the relative contributions of each spectral estimate to the total signal. Figure 5 shows both the new spectral estimates as well as their contributions in each spectrum. Spectra 1−33 correspond to experiment 1, and those from 34−95 correspond to experiment 2.

The relative concentration profiles are, at first glance, somewhat surprising. Indeed, one would expect a monotonic decrease in the signals of the reagents as a function of time, and a monotonic increase in the products as a function of time. In part, the unexpected concentration profiles are believed to be the result of the significant density differences in the compounds present coupled with the agitation/fluidization of the solid particles that occurs in the Linkam holder. Indeed, the gas flow is vertical and passes through the solid particle bed. This probably results in some stratification of the particles according to their densities over time. The total signal contribution of each component to the overall measurements is presented in Table 2.

4.2.3.3. Further Considerations of Phosphate Vibration. Although the partial range analyses provided quite adequate spectral estimates and relative concentration profiles, the phosphate vibration in the ZrP spectral estimate is considerably broader than the other vibrations and therefore requires further consideration. Additional BTEM analyses were made on the very restricted interval of 1000−1200 cm^{-1} (not shown here). Although there is still some noise in the new spectral reconstructions, it becomes evident that the broad band seen for ZrP in Figure 5 is in fact a superposition of two signals, with maxima at 1087 and 1091 cm^{-1}. A pure reference of ZrP shows a maximum only at 1091 cm^{-1}. The origin of the superimposed signal with a band maximum at

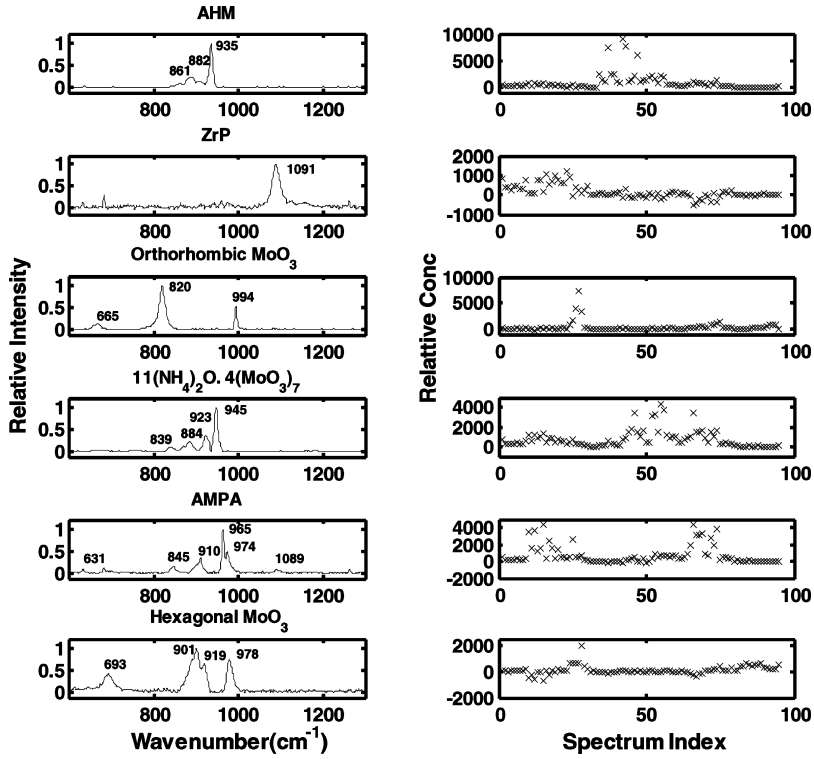

Figure 5. Partial range BTEM spectral estimates for the inorganic compounds as well as their relative contributions to experimental signal intensity.

Table 2. The Total Signal Contribution of Each Normalized Pure Component Spectrum to the Overall Measurements from 95 in Situ Spectra

pure component	contribution to total signal intensity (%)
AHM	17.9
ZrP	8.4
orthorhombic MoO_3	11.0
hexagonal MoO_3	9.5
$11(NH_4)_2O\cdot4(MoO_3)_7$	19.5
AMPA	27.2

1087 cm^{-1} is not entirely clear, but it apparently arises due to colinearity with some other signal. In this regard, it can be noted that AMPA has a phosphate vibration at ca. 1089 cm^{-1}.

4.3. Further Comparison of Experiments 1 and 2. Experimental runs 1 and 2 differ due to the initial AHM/ZrP ratios used. In the first experiment, the ratio was 0.7, and in the second experiment, the ratio was 1. These different initial compositions appear to have affected the formation and stability of the desired product, AMPA.

In experiment 1, the signals from AMPA start to increase at ca. 250 °C, go through a maximum, and then approach zero at ca. 400 °C. During the same period, the signals of the observable intermediate $11(NH_4)_2O\cdot4(MoO_3)_7$ also increase and then decrease. As the signals of AMPA and $11(NH_4)_2O\cdot4(MoO_3)_7$ start to decrease, the signals of both hexagonal and orthorhombic MoO_3 increase (see spectral numbers 20−25 in Figure 5). This implies that the degradation of AMPA (and perhaps $11(NH_4)_2O\cdot4(MoO_3)_7$) to MoO_3 at prolonged exposure at 400 °C.

Many of the observations from experiment 2 are similar to those from experiment 1. For example, the signals from AMPA start to increase at ca. 200 °C, go through a maximum, and approach zero at ca. 350 °C. The signals of the observable intermediate $11(NH_4)_2O\cdot4(MoO_3)_7$ increase at a lower temperature, 115 °C, go through a maximum, and then approach zero at ca. 350 °C. As before, the signals of both hexagonal and orthorhombic MoO_3 increase as the signals of AMPA and $11(NH_4)_2O\cdot4(MoO_3)_7$ start to decrease (see spectral number 70−80 in Figure 5).

Experiments 1 and 2 are also similar because the fate of zirconium could not be determined from the Raman measurements. Indeed, in both experiments, the signals from ZrP entirely disappear, but no signals from a new zirconium-containing phase appear. Since the raw experimental reaction spectra (Figure 2) show a pronounced increase in the background signal (average of 2000−5000 counts per second), it is possible that the zirconium (or a new zirconium compound) is present in an amorphous state, and no distinct Raman bands are observed. Therefore, the overall reaction for the formation of AMPA (up to ca. 300 °C) appears to be best expressed as

$$3(NH_4)_2O\cdot(MoO_3)_7\cdot4H_2O(s) + ZrP_2O_7(s) \rightarrow (NH_4)_3PMo_{12}O_{40}\cdot4H_2O(s) + 9MoO_3(s) + 3NH_3(g) + 8H_2O + 1.5H_2(g) + ZrPOx \text{ (amorphous solid)}$$

Previous work has been reported on the solid-state degradation of AHM alone. Murugan and Chang[29] reported the thermal degradation of AHM, initially to $11(NH_4)_2O\cdot4(MoO_3)_7$ and $7(NH_4)_2O\cdot4(MoO_3)_7$ and finally orthorhombic MoO_3, at ca. 385 °C. The present experiments involving AHM and ZrP as starting materials are consistent with the aforementioned observation. Orthorhombic molybdenum oxide MoO_3 is the most stable molybdenum-containing compound at higher temperatures.

The differences in the initial AHM/ZrP ratios for experiments 1 and 2, as well as the differences in the thermal behavior of the two systems, require further consideration. At the lower AHM/ZrP ratio of 0.7, the degradation of AMPA appears to occur at 400 °C. At the higher AHM/ZrP ratio of 1, the degradation of AMPA appears to occur starting at 350 °C. There appears to be an optimal AHM/ZrP ratio for maximum AMPA formation. Indeed, Bondareva et al.[39] also expressed a similar opinion that, for wet impregnation methods, any excess of Mo or P above the stoichiometric composition (above ca. 0.7) required by the heteropolyacid salt could lead to the formation of the corresponding oxides. For example, degradation of AMPA to MoO_3 can be expressed as below:

$$2[(NH_4)_3PMo_{12}O_{40}\cdot 4H_2O(s)] \rightarrow 24MoO_3(s) + P_2O_5(s) + 6NH_3(g) + 11H_2O$$

The present temperature-ramped experiments using AHM and ZrP as precursors show that the solid-state reaction should be conducted with a ca. 0.7 ratio of AHM and ZrP and should be terminated at ca. 350 °C in order to maximize the yield of the desired product $(NH_4)_3PMo_{12}O_{40}\cdot 4H_2O$. Above this temperature, degradation to MoO_3 occurs.

5. Conclusions

The formation of AMPA during the solid-state reaction between AHM and ZrP was observed using in situ Raman spectroscopy for the first time. This solid-state procedure avoided the use of the more commonly needed pH control during synthesis, particularly wet impregnation approaches. Six pure component spectra of inorganic compounds were reconstructed using the BTEM algorithm, and the contributions of the individual signal intensities of each constituent to the total measured signal intensity were determined (range: 8.4−27.2%). By combining in situ Raman spectroscopy and BTEM curve resolution, it was possible to identify a transient intermediate, $11(NH_4)_2O\cdot 4(MoO_3)_7$, during the solid-state synthesis. This latter finding helps to explain some of the selectivity and side-product observations. By studying the reaction until 400 °C, it was possible to confirm that good yield of the desired product, AMPA, is achieved at 350 °C, and any further temperature increase leads to its degradation.

With regard to the signal processing issues, it was found that full-range spectral analyses were possible. However, the quality of these spectral estimates could be considerably improved by analyzing the data over a slightly more restricted spectral range. The improvement in spectral estimation is a direct result of minimizing the integration of noise which occurs when large spectral ranges are used. The present combined spectroscopic and chemometric approach appears applicable to other solid-state syntheses as well.

IC801609D

(39) Bondareva, V. M.; Andrushkevich, T. V.; Plyasova, L. M.; Maksimovskaya, R. I.; Chumachenko, N. N. *React. Kinet. Catal. Lett.* **1998**, *63*, 201.